Photo-driven self-excited hydrogel oscillators

Chen Xuan[1,†,‡], Yu Zhou[1,†], Yusen Zhao[2], Ximin He[2], Lihua Jin[1,*]
[1] Department of Mechanical and Aerospace Engineering, University of California, Los Angeles, 90095, USA
[2] Department of Materials Science and Engineering, University of California, Los Angeles, 90095, USA

Abstract
Stimuli-responsive materials have been designed for self-sustained soft robots. Using a photo-thermally responsive hydrogel cantilever as a model system, this paper investigates its mechanism of and energy flow in self-excited oscillation under a constant light source. Based on an analytical model, we show that a periodic photo moment, produced by non-uniform water concentration across the cantilever's thickness driven by diffusion, is imposed on the cantilever by the ever-switching light incidence between the top and bottom surfaces. The synergy between the photo moment and oscillation ensures positive work input to the cantilever when the diffusion time scale is comparable to the period of free oscillation. When the input energy is higher than the damping energy, the oscillation amplitude increases, while when the input energy is lower, the amplitude decreases. Based on dimensional energy analysis, we determine the stable oscillation amplitude, and construct phase diagrams for the increase and decrease of the oscillation amplitude, which are further confirmed experimentally. A mass-spring-damper system subjected to a displacement-dependent excitation force is developed to investigate the features in generalized self-excited oscillating systems. This work lays a solid foundation for understanding self-excited oscillation, and provides design guidelines for self-sustainable soft robots.

I. Introduction

Stimuli-responsive materials can alter their shapes, volumes or functions in response to external stimuli, such as heat, light, chemical, or electrical fields [1]. Building soft robots with stimuli-responsive materials is the most promising strategy to achieve their miniaturization and untethered locomotion. However, to accomplish sustainable motions of such soft robots, complex control of external stimuli is usually essential [2–6]. An emergent trend is designing self-sustainable soft robots that can maintain motions under simple or constant external stimuli through the sophisticated interaction between stimuli-responsive materials and external stimuli [7–15].

One of the most useful self-sustainable motions is self-excited oscillation, i.e. autonomous oscillation of stimuli-responsive materials without artificially switching on/off external stimuli [8,16–21]. It is especially inspired by biological rhythms, i.e. oscillatory changes of chemical or mechanical functions, in living organisms; examples include circadian clocks and heartbeats. A hydrogel with its polymer network undergoing a non-equilibrium oscillatory reaction, such as Belousov–Zhabotinsky reaction, is capable of autonomous swelling and deswelling cycles [22,23]. A humidity-responsive material in a

† C.X. and Y.Z. contributed equally to this work.
‡ Current address: Department of Foundational Mathematics School of Science, Xi'an Jiaotong-Liverpool University, Suzhou 215123, China
* Corresponding authors: lihuajin@seas.ucla.edu

humidity gradient can bend and oscillate [24]. An alternative strategy is to utilize the fact that deformation of photo-responsive materials can alter or even block light incidence [13,25], which drives the recovery of the deformation, inducing a cyclic response. Autonomous oscillation [16,26–29] and continuous wave propagation [30] have been achieved and modeled [7,31–33] in photo-responsive liquid crystal elastomers and hydrogels under constant light radiation. Although the process of the self-excited oscillation is relatively intuitive, it is not clear how the autonomous oscillation is maintained through the sophisticated interaction and energy flow between the stimuli-responsive materials and external stimuli, and how material and geometric parameters govern the stable oscillation behavior.

Here we investigate a photo-driven self-excited hydrogel oscillator that can autonomously vibrate under constant light, and determine its stable oscillation behavior by examining its energy flow (Fig. 1). A hydrogel is a polymer network dispersed in water. In a photo-thermally responsive hydrogel, heating due to photo-absorption can trigger a chemical potential increase of the water molecules, and induce deswelling of the hydrogel. When the photo-thermally responsive hydrogel cantilever (Fig. 1a) deviates from its horizontal rest position, the light is shined on one of its surfaces, driving water molecules to diffuse out of the hydrogel and forming a concentration gradient, which produces a moment to bend the cantilever towards the opposite direction. Since the moment is photo-induced, we simply call it photo moment. Once the cantilever deflects beyond the rest position, the light relocates onto the opposite surface, creating an additional negative photo moment to bend the cantilever back to the original side. This process can go on periodically under an ever-switching photo moment. Our system falls into the categories of non-smooth piecewise systems and non-harmonic dynamically shifted oscillators [34–37]. We will analyze the work input into the hydrogel through its sophisticated interaction with the constant light, and the damping energy output to the external water. Balance of the work input and damping energy will allow us to determine the stable oscillation amplitude, which is governed by several dimensionless material and geometric parameters. We will theoretically and experimentally show that oscillation with a different amplitude will autonomously increase or decrease its amplitude until reaching the stable value. A simplified mass-spring-damper model is further developed to manifest the mechanism of and energy flow in generalized self-excited oscillating systems.

II. Theory for self-excited hydrogel oscillators

We model vibration of a hydrogel cantilever of length L and thickness h in water triggered by constant light radiation in the axial direction (Fig. 1a). The cantilever is assumed to undergo a small deflection $w(x,t)$ with respect to its equilibrium free swelling state, as a function of the coordinate x and time t, governed by

$$\rho A\frac{\partial^2 w}{\partial t^2}+c\frac{\partial w}{\partial t}+EI\frac{\partial^4 w}{\partial x^4}=EI\frac{\partial^2\left(1/R_{ph}\right)}{\partial x^2}, \tag{1}$$

with density ρ, cross section area A, Young's modulus E, and area moment of inertia I. The second term assumes that the damping force on a unit length of the hydrogel is proportional to the deflection velocity, with the damping coefficient c, due to the drag from the water. With the left end clamped and the right end free, the boundary conditions are

$$w(0,t)=\frac{\partial w}{\partial x}(0,t)=0,\ \frac{\partial^2 w}{\partial x^2}(L,t)=\frac{\partial^3 w}{\partial x^3}(L,t)=0. \tag{2}$$

The term on the right hand side of Eq. (1) is the distributed load produced by the photo moment EI/R_{ph}, where R_{ph} is the spontaneous radius of curvature in the illuminated region $x\in[0,d_{\mathrm{ph}}]$ arising from a gradient of photo-driven deformation through the thickness. This causes local bending of the beam in the region $x\in[0,d_{\mathrm{ph}}]$. The spontaneous curvature can be obtained as (Appendix A)

$$1/R_{\mathrm{ph}}=-\int_A \varepsilon_{\mathrm{ph}}(z)z\mathrm{d}A\Big/I, \tag{3}$$

where $\boldsymbol{\varepsilon}_{\mathrm{ph}}(z)=\mathrm{diag}\left(\varepsilon_{\mathrm{ph}}(z),\varepsilon_{\mathrm{ph}}(z),\varepsilon_{\mathrm{ph}}(z)\right)$ is the the spontaneous photo-strain at the position z induced by the photo-driven diffusion. Assuming the hydrogel undergoes pure bending with respect to the non-irradiated state, the photo-strain is related to the water concentration C through $\varepsilon_{\mathrm{ph}}(z)\doteq$ $)+1)/(\Omega C_0+1)-1]/3$, where C_0 is the water concentration in hydrogel when the hydrogel is in equilibrium with pure water without radiation.

We model the photo-thermally driven water migration as a one-dimensional diffusion problem along the thickness [38,39]

$$\frac{\partial C}{\partial t}=\frac{D}{k_{\mathrm{B}}T}\frac{\partial}{\partial z}\left(\frac{C}{\lambda_z^2}\frac{\partial \mu}{\partial z}\right), \tag{4}$$

where λ_z is the stretch ratio of the hydrogel in the current state with respect to its non-radiated equalibrium state, μ is the chemical potential of the water molecules in the hydrogel (defined in Appendix A), and D is the diffusivity of water molecules in the hydrogel. Although it should be noted that hydrogels may have different diffusion kinetics for swelling and deswelling [40], here in our theory, we just use Eq. (4)~~(4)~~ to describe both swelling and deswelling. To capture that water molecules diffuse out of the hydrogel through the illuminated surface, we simply assume the light changes the chemical potential of the water molecules on the illuminated boundary, i.e. apply $\mu=-\mu_{\mathrm{ph}}<0$ on the illuminated surface and $\mu=0$ on the non-illuminated surface.

The photo-induced bending curvature Eq. (3)~~(3)~~ produces a photo moment in the region $x\in[0,d_{\mathrm{ph}}]$ in Eq. (1). In the meantime, $\varepsilon_{\mathrm{ph}}(z)$ is governed by the diffusion equation (4). Solving Eqs. (1) and (4)~~(4)~~ together, we can fully determine the spatiotemporal response of the photo-driven hydrogel oscillator. Both equations (1) and (4)~~(4)~~ are solved by the forward-time central-space finite difference method. The solution of Eq. (4)~~(4)~~ will enable one to calculate the spontaneous radius of curvature by Eq. (3)~~(3)~~ as an input to the right hand side of Eq. (1) at every time step. In such a coupling process between the beam vibration and water diffusion, there are three time scales, the viscous relaxation time scale $t_c=\rho A/c$, the inertia time scale $t_{\mathrm{i}}=\sqrt{\rho AL^4/EI}$ and the diffusion time scale $t_{\mathrm{d}}=h^2/D$, arising from

Eq. (1) and Eq. (4)~~(4)~~, which leads to two time-scale ratios t_i/t_c and t_i/t_d. Clearly, the time-scale ratio t_i/t_c represents the normalized damping factor, indicating how large the damping force is compared to the inertia force, and t_i/t_d represents the normalized diffusivity, indicating how fast the water diffuses compared to the vibration velocity. We shall show these two normalized parameters can greatly influence the vibration behavior.

III. Results

A. Amplitude increase and decrease

A cantilever starting from the horizontal position with an initial velocity, $v_0(x)=\dot{\ell}$, vibrates under inertia and radiation. Following our previous work [7], parameters for all simulations are set as $d_{\mathrm{ph}}/L=1/20$, $N\Omega=10^{-3}$, $\chi=0.3$, $\mu_{\mathrm{ph}}/k_{\mathrm{B}}T=3\times10^{-4}$, $v_0(L)t_i/L=-1/3$ and $L/h=10$, unless otherwise stated. Two types of vibration behavior are observed: the amplitude of the deflection decreases (Fig. 1b and Movie S1 within the Supplemental Material [41]) or increases (Fig. 1c and Movie S2 within the Supplemental Material [41]) over time, and saturates when time is long enough for both cases. Although the light radiation is constant, it passively switches its incident spot piecewise between the top and bottom surfaces in the same period as the oscillation, forming a photo-driven self-excited oscillation. Whether the amplitude decreases or increases depends on different parameters, including the normalized damping factor, the normalized diffusivity, the geometry, the radiation-induced chemical potential decrease, and the initial velocity. As a demonstration, we only vary the length-to-thickness ratio ($L/h=5$ for Fig. 1b and $L/h=10$ for Fig. 1c), and detailed phase diagrams for the increase and decrease of the oscillation amplitude will be provided later. The angular frequencies in both cases are close to the classical limit of cantilever vibration, $3.5/t_{\mathrm{i}}$, indicating that the bending shape is roughly in the 1st mode of cantilever vibration (Figs. 1b and c).

B. Experiments

To experimentally verify the existence of both cases of amplitude increasing and decreasing, we demonstrate oscillation of a Poly(N-isopropylacrylamide) (PNIPAAm) hydrogel (Fig. 1d), where gold nanoparticles (AuNPs) are added to incorporate the photo-thermal effect [7]. To fabricate hydrogel pillars, the AuNPs/PNIPAAm precursor solution was prepared with 40 wt% NIPAAm monomer, 1.5 wt% N,N′-methylenebis(acrylamide) (BIS), 0.5 vol% Darocur 1173, and 0.5 wt% AuNPs in dimethyl sulfoxide, and then cured in a PDMS mold under UV light for 80 s. Details of the synthesis and characterization of the gold nanoparticles can be found in the literature [7]. Pillars with a circular cross-section of two different diameters were fabricated. The as-prepared diameters were 0.71 mm and 0.50 mm, and the corresponding equilibrium swelling diameters were 0.9 mm and 0.56 mm, respectively. After the hydrogels reach equilibrium in water, the Young's modulus is measured to be 6.3kPa. Upon exposure to a green laser (532 nm and $\geqslant$ 200 mW with the beam diameter of 1 mm), the hydrogel is heated on the front surface due to photo absorption of the gold nanoparticles. Once the temperature reaches the lower critical solution temperature (LCST) of PNIPAAm (~32℃), water molecules diffuse out, which creates a concentration gradient in the thickness direction, and bends the initially vertical hydrogel

pillar to the horizontal direction, followed by autonomous oscillation of the effective cantilever about the horizontal plane (Fig. 1d). For a hydrogel cantilever of a length L = 17 mm, the amplitude decays over time when the diameter is h = 0.9 mm (L/h = 18.9, Fig. 1e and Movie S3 within the Supplemental Material [41]), while the amplitude grows over time when the diameter is h = 0.56 mm (L/h = 30.4, Fig. 1f and Movie S4 within the Supplemental Material [41]).

It should be noted that there are some differences between the theoretical modeling and the experiment. Our goal is to build a generic framework to study the self-excitation of hydrogel beam structures and understand the mechanism of the self-excitation. The experiment is a demonstration of the self-excitation phenomenon. In the experiment, the hydrogel pillar is bent from the initially vertical position to the horizontal direction, while a horizonal hydrogel cantilever is modelled in the theory. The experimental setup is to give a substantial initial speed of the hydrogel beam as it hits the horizontal position. Our theory starts from a horizontal position with an input initial speed, so the theory and experiment are consistent. We skip the initial process from the vertical to horizontal position in the theory since that is not the essential part we are interested in. In the experiment, when the hydrogel is at the largest downward deflection, the light is almost blocked by its tip, leading to different boundary conditions between the top and bottom surfaces. Ideally, when the beam is thin enough, the light could be shined on the corner of the top surface, resulting in better agreement between the experiment and theory. On the other hand, our theory is also capable of modeling the case when the light is blocked by the tip of the hydrogel by setting the chemical potential boundary condition of the top surface to be always zero.

C. Without damping

To understand the requirements for a self-excited oscillation, we first investigate the effect of the normalized diffusivity for an ideal scenario without damping. When the diffusion time scale is comparable to the inertia time scale ($t_\mathrm{i}/t_\mathrm{d}=1$ in Fig. 2a), the vibration amplitude increases over time. The amplitude grows without saturation due to lack of damping. The photo curvature changes in a periodic manner, but with about $\pi/2$ phase lag with respect to the tip deflection due to the non-equilibrium diffusion process (Fig. 2a). The photo curvature is a consequence of inhomogeneous distribution of water concentration C and photo strain ε_ph through the thickness direction (Fig. 2c). The work done to the cantilever by the light over time t can be calculated as $W_l(t)=\int_0^t EI\dot{\epsilon}$, where $\dot{\epsilon}$ is the change rate of the angle at $x=d_\mathrm{ph}$ (Fig. 2b). The irregular time response of $\dot{\epsilon}$ is due to the vibration with multiple modes. When the cantilever strokes downward from the horizontal position, the radiation spot leaves the bottom surface and moves onto the top surface, and the photo curvature reaches the valley (insets of Fig. 2a). The radiation on the top surface decreases the water concentration in its vicinity, and increases the photo curvature. Due to diffusion, it takes some time (less than a quarter period) for the curvature to reach zero. Considering that $\dot{\epsilon}$ is negative, the photo moment does positive and negative work to the cantilever, before and after the curvature reaches zero, respectively (insets of Figs. 2a and b). After the tip deflection reaches its valley, $\dot{\epsilon}$ becomes positive and the photo moment does positive work to the cantilever again. When the cantilever hits the horizontal line, the irradiated spot switches to the bottom surface, and the photo curvature reaches its peak. Therefore, within the half vibration period, the total work done

to the cantilever first increases, then decreases and increases again (insets of Fig. 2b); the total work follows the similar trend within the next half period. Due to the synergy of the photo moment and the change rate of the bending angle, the net work done to the system over a period is positive, which leads to the increase of the deflection amplitude. When the cantilever just starts to vibrate, the water concentration only decreases in the outer layer in response to the radiation (the black curve in Fig. 2c). In the later cycles, the outer layer on the side illuminated shrinks more, and the outer layer without radiation partially re-swells. The shrinkage zone goes deeper and deeper into the cantilever (the red curve in Fig. 2c), and eventually saturates.

When the diffusion is much slower than the vibration, the beam vibrates periodically with a fixed amplitude ($t_i/t_d = 0.0001$ in Fig. 2d), as the photo moment built up in a time scale of inertia is so small that the work done to the cantilever is negligible. When the diffusion is much faster than the vibration, the photo curvature acts like a step-function excitation (Appendix B). Therefore, once the cantilever goes below the horizontal line, the photo curvature immediately becomes positive, so the positive and negative work cancel each other, and vice versa. Also since the diffusion is fast, it perturbs the regular bending mode of the cantilever, leading to the excitation composed of multiple bending modes other than the 1st mode. In this case, the beam will block the light, violating the assumption that the beam is shined in the region $x \in [0, d_{\mathrm{ph}}]$. Therefore, in our later study, the normalized diffusivity will be limited to less than 20. Below this limit, a higher normalized diffusivity leads to a larger photo moment and higher work input, which increases the amplitude of the deflection faster (Fig. 2e).

D. With damping

Next, we consider self-excited hydrogel oscillators subjected to damping. Given different normalized damping factors, the tip deflection amplitude A_w either increases or decreases over time and then saturates (Fig. 3a), the saturated value is called the stable amplitude. As the normalized damping factor increases, the stable amplitude decreases (Fig. 3a), and the diminishing amplitude causes the angular frequency $\omega = 2\pi/T_p$ to increase (Fig. 3b), where T_p is the period of the vibration. The normalized diffusivities $t_{\mathrm{i}}/t_{\mathrm{d}}$ within certain range show little effect on the vibration frequency (Fig. 3b). If the normalized diffusivity is further increased, i.e. $t_{\mathrm{i}}/t_{\mathrm{d}} = 100000$, the vibration frequency increases (Appendix B). The energy loss due to damping over time t can be calculated as $W_c(t) = \int_0^t \int_0^L c\dot{\mathrm{}}$. As a result, when the cantilever just starts to vibrate, the system with a larger normalized damping factor exhibits higher energy dissipation. However, when the vibration reaches the steady state, it has lower energy dissipation due to a lower stable amplitude (Fig. 3c), implying the energy loss is influenced by both the vibration amplitude and damping factor.

E. Scaling analysis for energy flow

We further investigate the effect of other parameters on the self-excited oscillation, and conduct scaling analysis for the work input and energy dissipation to construct a phase diagram for the increase and decrease of the oscillation amplitude (Figs. 4 and 5). The

radiation does work $W_{lp} = \int_0^{T_p} EI\dot{\kappa}$ to the cantilever over a period. Since the bending angle scales as $\theta \sim A_w / L$, the work done to the cantilever can be rewritten as $W_{lp} \sim EIA_w / \left(R_{\mathrm{ph}} L\right)$. Using Eq. (3)(3) and assuming a linear distribution of spontaneous photo strain along the thickness direction, we find that the spontaneous radius of curvature scales with the square of the thickness, $R_{\mathrm{ph}} \sim h^2$, is inversely proportional to the diffusion thickness $\sqrt{DT_p}$, and nonlinearly depends on the photo chemical potential $\mu_{\mathrm{ph}} / k_{\mathrm{B}} T$ (Appendix C). Therefore, the work per period can be further rewritten as $W_{lp} \sim f\left(\mu_{\mathrm{ph}} / k_{\mathrm{B}} T\right) EIA_w \sqrt{DT_p} / Lh^2$, with f an increasing function of $\mu_{\mathrm{ph}} / k_{\mathrm{B}} T$. As Fig. 3b shows, the period T_p can be further expressed as $t_i / g\left(t_i/t_d, t_i/t_c\right)$, where g is a weak function of t_i/t_d and t_i/t_c, and we can treat it as a constant. Combining with the diffusion time scale $t_{\mathrm{d}} = h^2 / D$, we have

$$W_{lp} \sim f\left(\mu_{\mathrm{ph}} / k_{\mathrm{B}} T\right)(1/h)\left(EI\sqrt{t_i/t_d}\right)\left(A_w/L\right). \tag{5}$$

In the meantime, the cantilever loses energy over a period due to damping can be calculated by $W_{cp} \sim \int_0^{T_p} \int_0^{L} c\dot{w}$, where the deflection w scales with the tip amplitude A_w, so we have

$$W_{cp} \sim \quad _p \sim (1/t_i)(cL^3)\left(A_w/L\right)^2. \tag{6}$$

Consistent with the classical self-excited oscillation [42], our numerical results indeed show that under various damping factors and geometric parameters the normalized work done to the cantilever $W_{lp} h / \left(EI\sqrt{t_i/t_d}\right)$ is proportional to the normalized tip amplitude A_w/L with the fitted slope $k_l = 3.793 \times 10^{-3}$ (Fig. 4a), and the normalized damping energy $W_{cp} t_i / cL^3$ is proportional to the square of the normalized tip amplitude $\left(A_w/L\right)^2$ with the fitted slope $k_c = 2.895$ (Fig. 4b). To further compare the work input and energy dissipation within a period, we normalize both of them by cL^3/t_i, which are equal to $k_l (L/h)\left(A_w/L\right)\sqrt{t_i/t_d}\,/\left(t_i/t_c\right)$ and $k_c \left(A_w/L\right)^2$, respectively, and are plotted as functions of A_w/L (Fig. 4c). The results are based on the parameters $t_i/t_c = 1$, $t_i/t_d = 1$ and $L/h = 10$, which have not been used for the fitting in Fig. 4a and b. The intersection of the two curves determines the stable amplitude, and it agrees well with the results obtained in Fig. 3a. By using $W_{lp} = W_{cp}$, we obtain the scaling of the stable amplitude

$$A_w/L \sim \quad \sim \quad \rho^{\frac{3}{4}} E^{\frac{1}{4}} D^{\frac{1}{2}} C^{-1}. \tag{7}$$

Clearly, a higher normalized diffusivity t_i/t_d, higher length-to-thickness ratio L/h or lower normalized damping factor t_i/t_c increases the normalized work $W_{lp}t_i/cL^3$, and therefore, increases the stable amplitude (Fig. 4c).

Depending on whether the initial amplitude A_0 is smaller or larger than A_w, the amplitude increases or decreases to reach A_w. Since the initial amplitude scales with the initial velocity $A_0/L \sim$ ~ , the boundary between amplitude increase and decrease $A_0/L = A_w/L$ gives

$$v_0(L)t_i/L \sim f\left(\mu_{ph}/k_BT\right)\frac{L}{h}\frac{\sqrt{t_i/t_d}}{t_i/t_c}. \quad (8)$$

The decisive dimensionless material and geometric parameters for the phase boundary are μ_{ph}/k_BT, $v_0(L)t_i/L$, t_i/t_d, t_i/t_c and L/h. Consistent with Eq. (8), the numerical results show linear boundaries between the amplitude increase and decrease regions in the phase plane of t_c/t_i and $v_0(L)t_i/L$ (Fig. 4d), the phase plane of t_i/t_c and $\sqrt{t_i/t_d}$ (Fig. 4e), and the phase plane of t_i/t_c and L/h (Fig. 4f). Fig. 4g shows a nonlinear boundary between the amplitude increase and decrease in the phase plane of t_i/t_c and μ_{ph}/k_BT. The successful prediction of the phase boundary further verifies the stable amplitude Eq. (7)~~(7)~~.

Now let us use the scaling analysis to examine the oscillation behavior of the two hydrogel beams in the experiment. The inertia time scale $t_i = \sqrt{\rho AL^4/EI}$ can be calculated as 0.51 s for the thick beam, and 0.82 s for the thin beam, given $\rho = 10^3 kg/m^3$. The corresponding frequencies can be approximated as $\omega \approx 3.5/t_i = 6.84$ rad/s and 4.26 rad/s, respectively. These agree with the experimentally observed frequencies 6.28 rad/s and 1.19 rad/s, indicating the simplification of the hydrogels as cantilever beams vibrating in the 1st mode is reasonable. The deviation is because in the experiment the end of a horizontal hydrogel is not fixed, but connected to a vertical portion of the hydrogel, which has the freedom to vibrate itself; a thinner hydrogel pillar corresponds to a weaker boundary constraint, and therefore, a lower frequency. To further estimate the viscous relaxation time scale t_c in the experiment, we have approximated the damping coefficient c to be $4.45 \times 10^{-3} Pa \cdot s$ (Appendix D), and as a result, $t_c = \rho A/c = 0.14$ s for the thick beam, and $t_c = 0.055$ s for the thin beam. By using the diffusivity of our hydrogel $D = 10^{-8}$ m^2/s, we can calculate $t_d = h^2/D = 81$ s for the thick beam, and $t_d = 31.36$ s for the thin beam. Consequently, the normalized diffusivity t_i/t_d is 6.3×10^{-3} and the normalized damping factor t_i/t_c is 3.58 for the thick beam, while $t_i/t_d = 2.62 \times 10^{-2}$ and $t_i/t_c = 14.86$ for the thin beam. The length-to-thickness ratios for the thick and thin beams in the experiment are L/h = 18.9 and 30.4, respectively. The spontaneous photo strain on the shined surface $\varepsilon_0 = f\left(\mu_{ph}/k_BT\right)$ (Appendix C) for PNIPAAm hydrogels can be estimated as 0.2. Using Eq. (8)~~(8)~~, we can calculate the normalized stable amplitudes

$f\left(\mu_{\text{ph}}/k_{\text{B}}T\right)\frac{L}{h}\frac{\sqrt{t_i/t_d}}{t_i/t_c}$ are comparable for the thick and thin beams, and are 0.084 and 0.066, respectively. However, as their normalized initial amplitudes $v_0(L)t_i/L$ are very different, and are 0.12 and 9.7×10^{-3} for the thick and thin beams, respectively, this explains why we observe amplitude decrease in the thick beam and amplitude increase in the thin beam. Note that a pre-factor is needed on the right hand side of the scaling relation in Eq. (8)~~(8)~~ to equate the initial amplitude to the stable amplitude. The pre-factor obtained from our numerical calculation is about 0.1, which makes the stable amplitude of the thin beam to be slightly smaller than the initial amplitude. Considering the simplicity of the scaling analysis, we can still claim its success in predicting the amplitude variation of the self-excited oscillation. Since the damping from water is high, it is usually challenging in observing autonomous vibration of hydrogels in water. In our experiments, the relatively high diffusivity of water in the hydrogels is the enabling factor for the self-excited oscillation.

F. Mass-spring-damper system with non-smooth excitation force

We further propose a simplified single-degree-of-freedom mass-spring-damper system to shed light on the various features we observe in the photo-driven hydrogel oscillator. Analogous to the photo moment, a position and time dependent forcing term F is added as an excitation force

$$\begin{cases} m\ddot{x} = -\alpha\dot{x} - kx + F, \\ \dot{F} = \left[F_\infty \operatorname{sgn}(x) - F\right]/\tau, \end{cases} \tag{9}$$

where m is the mass, α is the damping factor, k is the stiffness of the spring, $\dot{}$ denotes time derivative d/dt, F_∞ is an excitation force constant, and $\operatorname{sgn}(x)=|x|/x$. The sgn term, as a non-smooth piecewise term, mimics the ever-switching light source in the hydrogel system. The excitation force F changes exponentially in time, with a characteristic time scale τ featuring a non-equilibrium process, such as diffusion or reaction. This simplified system, originating from the prototypical systems of dynamically shifted oscillators [34–37], serves as a good approximation for us to understand the response-dependent excitation of the hydrogel cantilever. Similar to the hydrogel oscillator, we have three time scales, including the viscous relaxation time scale m/α, the inertia time scale $\sqrt{m/k}$, and the excitation time scale τ, which defines two time-scale ratios, the normalized damping factor $\alpha/\sqrt{km}$ and the normalized excitation velocity $\sqrt{m/k}/\tau$.

First consider the ideal scenario where there is no damping α = 0. When the excitation time scale is comparable to the inertia time scale, $\sqrt{m/k}/\tau=1$, the vibration amplitude increases as a function of time and the trajectory on the phase plane diverges away from the initial position (Figs. 5a and d). When the excitation time scale is much larger than the inertia time scale, $\sqrt{m/k}/\tau=0.001$, the excitation force F is very small, and therefore, hardly affects the motion (Fig. 5b). The trajectory on the phase plane is close to a circle (Fig. 5e), indicating that the motion is similar to a harmonic oscillation. The amplitude can decrease (Fig. 5c) by adding a damping term $\alpha\dot{x}$ and the trajectory goes to a stable limit cycle on its phase plane (Fig. 5f). The simplified model predicts that a higher

normalized damping factor $\alpha/\sqrt{km}$ or a higher normalized excitation velocity $\sqrt{m/k}/\tau$ raises the frequency $\omega\sqrt{m/k}$ (Fig. 5g), which is consistent with the prediction of the hydrogel cantilever model. The increase of frequency can be observed from the limit cycle that changes from circular to oval shape, where the ratio between the amplitude of velocity and displacement increases (Figs. 5f, h and i).

We further study the work done and damping energy through scaling analysis. When the excitation velocity $\sqrt{m/k}/\tau$ is limited to less than 0.1, the normalized vabriation frequency is almost a constant. The work done by the force over a period is $W_f = \int_0^{T_p} F$ and can be rewritten as $W_f \sim \left(\sqrt{m/k}/\tau\right)\left(kA_x/F_\infty\right)$, where A_x is the vibration amplitude (Appendix E). The damping energy over a period is $W_\alpha = \int_0^{T_p} \alpha$ and can be rewritten as $W_\alpha \sim \left(\alpha/\sqrt{km}\right)\left(kA_x/F_\infty\right)^2$ (Appendix E). The numerical results prove that the normalized work $W_f/\left[\left(F_\infty^2/k\right)\left(\sqrt{m/k}/\tau\right)\right]$ is proportional to the normalized amplitude kA_x/F_∞ (Fig. 5j), and the damping energy $W_\alpha/\left[\left(F_\infty^2/k\right)\left(\alpha/\sqrt{km}\right)\right]$ is proportional to the square of the normalized amplitude $\left(kA_x/F_\infty\right)^2$ (Fig. 5k). By equating W_f and W_α, the stable amplitude is obtained as $kA_x/F_\infty \sim /\tau)/\left(\alpha/\sqrt{km}\right)$. Consistent with the prediction, the numerical results show that the stable amplitude is proportional to the excitation velocity and inversely proportional to the damping factor (Fig. 5l).

IV. Conclusions

This paper investigates the mechanism of and energy flow in photo-driven self-excited hydrogel oscillators, whose amplitude can increase or decrease with time under constant light radiation. When the hydrogel cantilever oscillates, the light incidence switches between the top and bottom surfaces, inducing a periodic photo moment with the same frequency as the oscillation. Since the photo moment is induced by an inhomogeneous distribution of water concentration through the thickness of the cantilever due to a non-equilibrium diffusion process, diffusion kinetics determines the temporal evolution of the photo moment. We find that when the diffusion time scale is comparable to the inertia time scale, the vibration of the cantilever can reach a significantly high amplitude, and remain stable. By analyzing the work done by radiation, it turns out that the synergy between the photo moment and oscillation ensures positive photo-mechanical energy pumped into the system every cycle to maintain self-excited oscillation overcoming damping. Based on dimensional analysis, we find that the work input is proportional to the vibration amplitude and the damping energy is proportional to the square of the amplitude. The balance of the work input and the energy dissipation determines the stable amplitude, which turns out to scale with the length-to-thickness ratio L/h, square root of the normalized diffusivity t_i/t_d and inverse of the normalized damping factor t_i/t_c, and depend on the radiation-induced chemical potential change of water $\mu_{ph}/k_B T$. By equating the initial and stable amplitude, we construct phase diagrams for the increase and decrease of the oscillation amplitude. To

further shed light on the self-excited oscillation, a simplified mass-spring-damper system with a single degree-of-freedom is proposed to understand the major features and energy flow in generalized self-excited oscillating systems. The effect of the material and geometric parameters on the vibration frequency, amplitude and energy of the hydrogel cantilever can be mostly reproduced by the simplified system. This study elucidates the design requirements of stimuli-responsive self-excited oscillators.

Acknowledgments

Y.Z. (Yu Zhou), and L.J. acknowledge the support from National Science Foundation through a CAREER Award No. CMMI-2048219, C.X., Y.Z. (Yu Zhou), and L.J. acknowledge the startup fund from the Henry Samueli School of Engineering and Applied Science at the University of California, Los Angeles (UCLA). Y.Z. (Yusen Zhao) and X.H. acknowledge AFOSR awards FA9550-17-1-0311, FA9550-18-1-0449 and FA9550-20-1-0344, and ONR awards N000141712117 and N00014-18-1-2314. The authors acknowledge Prof. Alan Garfinkel at UCLA for fruitful discussions on dynamic systems.

Equation Chapter (Next) Section 1

APPENDIX A: Theory for self-excited hydrogel oscillators

We model vibration of a hydrogel cantilever of length L and thickness h in water triggered by constant light radiation in the axial direction (Fig. 1a). The cantilever is assumed to undergo small deflection $w(x,t)$, as a function of the coordinate x and time t, governed by

$$\rho A\frac{\partial^2 w}{\partial t^2}+c\frac{\partial w}{\partial t}+EI\frac{\partial^4 w}{\partial x^4}=EI\frac{\partial^2\left(1/R_{ph}\right)}{\partial x^2}, \tag{A1}$$

with density ρ, cross section area A, Young's modulus E, and area moment of inertia I. The second term assumes that the damping force on unit length of the hydrogel is proportional to the deflection velocity, with the damping coefficient c, due to the drag from the water. The term on the right hand side of Eq. (A1)~~(A1)~~ is the distributed load produced by the photo moment EI/R_{ph}, where R_{ph} is the spontaneous radius of curvature in the region $x\in[0,d_{\mathrm{ph}}]$, with the width of the light beam d_{ph}, arising from a gradient of photo-driven deformation through the thickness, yet to be determined by solving a diffusion equation of water molecules. With the left end clamped and the right end free, the boundary conditions are

$$w(0,t)=\frac{\partial w}{\partial x}(0,t)=0,\ \ \frac{\partial^2 w}{\partial x^2}(L,t)=\frac{\partial^3 w}{\partial x^3}(L,t)=0. \tag{A2}$$

We model the diffusion of water molecules driven by a gradient of its chemical potential. The free energy density of a hydrogel consists of an elastic part and a mixing part, $W(\mathbf{F},C)=W_{\mathrm{net}}(\mathbf{F})+W_{\mathrm{mix}}(C)$. The elastic part considers the elastic energy of the polymer network as a function of the deformation gradient $\mathbf{F}$ per volume in the reference dry state [43,44]

$$W_{\mathrm{net}}(\mathbf{F})=\frac{1}{2}Nk_{\mathrm{B}}T\left[\mathrm{tr}\left(\mathbf{F}\mathbf{F}^{T}\right)-3-2\log\left(\det\mathbf{F}\right)\right], \tag{A3}$$

where N is the crosslink density of the hydrogel, k_{B} is the Boltzmann constant, and T is the temperature. The mixing energy density between the polymer and water per reference volume is a function of the water concentration C, the number of water molecules per unit reference volume [45]

$$W_{\mathrm{mix}}\left(C\right)=k_{\mathrm{B}}TC\left[\log\left(\frac{\Omega C}{1+\Omega C}\right)+\frac{\chi}{1+\Omega C}\right], \tag{A4}$$

where Ω is the volume of a water molecule, and χ is the Flory-Huggins interaction constant between the polymer and water. Both the polymer network and the water are assumed incompressible, so the volume change of the hydrogel is purely due to the migration of water molecules, $J=\det(\mathbf{F})=\Omega C+1$. The chemical potential of the water molecules in the hydrogel, μ, can be calculated as the following [38],

$$\mu=\frac{\partial W}{\partial C}+\Pi\Omega, \tag{A5}$$

where Π is the osmotic pressure, determined by the boundary conditions. When the hydrogel freely swells in water without constraints, the Cauchy stress

$$\boldsymbol{\sigma}=\left(\partial W/\partial\mathbf{F}\right)\mathbf{F}^{\mathrm{T}}/J-\Pi\mathbf{I} \tag{A6}$$

is zero, i.e. $\boldsymbol{\sigma}=0$, and the osmotic pressure can be determined as $\Pi_0=Nk_{\mathrm{B}}T\left(\lambda_0^{-1}-\lambda_0^{-3}\right)$, where λ_0 is the equilibrium isotropic stretch ratio with respect to the dry state, relating to the water concentration C_0 by $\lambda_0=\left(1+\Omega C_0\right)^{1/3}$. The equilibrium water concentration C_0 can be determined by $\mu\left(C_0\right)=0$ using Eq. (A5), i.e. the chemical potential of water in the hydrogel equals that of the pure water outside the hydrogel.

Absorption of light raises the temperature of the hydrogel on the irradiated surface, increasing the chemical potential of the water molecules, driving the water molecules to diffuse out of the hydrogel. Since the cantilever length is much larger than its thickness, water diffusion in the length direction can be neglected. We model the photo-thermally driven water migration as a one-dimensional diffusion problem along the thickness, with Z the reference coordinate in the thickness direction [38,39]

$$\dot{C}=\nabla\cdot\left(\mathbf{M}\cdot\nabla\mu\right), \tag{A7}$$

where $\mathbf{M}$ is the mobility tensor of water molecules in the hydrogel. To capture that the water molecules diffuse out of the hydrogel through the illuminated surface, we simply assume the light changes the chemical potential of the water molecules on the illuminated boundary, i.e. apply $\mu=-\mu_{\mathrm{ph}}<0$ on the illuminated surface and $\mu=0$ on the non-illuminated surface.

Next, we decompose the total deformation gradient $\mathbf{F}$ into $\mathbf{F}=\mathbf{F}'\mathbf{F}_0$, where $\mathbf{F}_0=diag\left(\lambda_0,\lambda_0,\lambda_0\right)$ maps the dry configuration to the wet non-irradiated one, and $\mathbf{F}'$ maps the wet non-irradiated configuration to the current irradiated configuration. We assume that the deformation arising from the swelling of the hydrogel with respect to the dry configuration is finite, while the deformation of oscillation under light radiation can be considered small. With linearized strain $\boldsymbol{\varepsilon}=\left(\mathbf{F}'+\mathbf{F}'^{\mathrm{T}}\right)/2-\mathbf{I}$, the Cauchy stress $\boldsymbol{\sigma}$ Eq. (A6) can be linearized as

$$\boldsymbol{\sigma} = \frac{2Nk_{\mathrm{B}}T}{\lambda_0}\boldsymbol{\varepsilon} + \left[\Pi_0(1-\mathrm{tr}\boldsymbol{\varepsilon}) - \Pi\right]\mathbf{I}. \tag{A8}$$

Then the diffusion equation (A7)~~(A7)~~ can be rewritten as

$$\frac{\partial C}{\partial t} = \frac{D}{k_{\mathrm{B}}T}\frac{\partial}{\partial z}\left(\frac{C}{\lambda_z^2}\frac{\partial \mu}{\partial z}\right), \tag{A9}$$

where $\lambda_z = 1+\varepsilon_z$ is the z component of $\mathbf{F}'$ after the linearization, and D is the diffusivity of the water molecules in the hydrogel. The photo-driven diffusion induces a spontaneous photo-strain, $\boldsymbol{\varepsilon}_{\mathrm{ph}}(z) = \mathrm{diag}\left(\varepsilon_{\mathrm{ph}}(z), \varepsilon_{\mathrm{ph}}(z), \varepsilon_{\mathrm{ph}}(z)\right)$ as a function of position z, where $\varepsilon_{\mathrm{ph}}(z) < 0$. We assume the hydrogel undergoes pure bending with respect to the non-irradiated state. Since the total volume change is due to diffusion, we have $\mathrm{tr}\boldsymbol{\varepsilon} = \mathrm{tr}\boldsymbol{\varepsilon}_{\mathrm{ph}} \doteq$ $)/(\Omega C_0+1)-1$, namely $\varepsilon_{\mathrm{ph}}(z) \doteq$ $)+1)/(\Omega C_0+1)-1]/3$. Based on pure bending, the total strain should be diagonal in its principal axes, $\boldsymbol{\varepsilon}(z) = \mathrm{diag}\left(\varepsilon_x(z), \varepsilon_y(z), \varepsilon_z(z)\right)$, where $\varepsilon_x(z)$ can be deemed linear in z, having a neutral plane at z_{n}, namely $\varepsilon_x(z) = (z_{\mathrm{n}} - z)/R$, with~~,~~ R ~~is~~ the radius of curvature of the beam. We will show how to determine z_{n} ~~and R_{ph}~~ using mechanical equilibrium hereafter. When diffusion just starts, there could be an infinitesimal curvature along the y direction alongside with the x curvature, but it will be easily suppressed by the dominant curvature $1/R$ as its magnitude develops [46]. Assuming there is no stress along y and z, we can solve for $\varepsilon_y = \varepsilon_z = \left[\mathrm{tr}\boldsymbol{\varepsilon}_{\mathrm{ph}} - (z_{\mathrm{n}} - z)/R\right]/2$, and the osmotic pressure $\Pi = \frac{Nk_{\mathrm{B}}T}{\lambda_0}(\mathrm{tr}\boldsymbol{\varepsilon} - \varepsilon_x) + \Pi_0(1-\mathrm{tr}\boldsymbol{\varepsilon})$. Inserting Π into Eq. (A8), we can determine the only non-vanishing stress component along x,

$$\sigma_x = \frac{3Nk_{\mathrm{B}}T}{\lambda_0}\left(\frac{z_{\mathrm{n}} - z}{R} - \varepsilon_{\mathrm{ph}}\right). \tag{A10}$$

Using the relationship $E = 3Nk_{\mathrm{B}}T/\lambda_0$ between the Young's modulus and the crosslink density, we can see Eq. (A10) is reminiscent of the 1D classical stress-strain relationship in the presence of a thermal strain, except the prefactor associated with pre-radiation swelling. Applying the force free condition to Eq. (A10)~~(A10)~~, namely $\int_A \sigma_x \mathrm{d}A = 0$, we get $z_{\mathrm{n}}/R = \int_A \varepsilon_{\mathrm{ph}}(z)\mathrm{d}A/A$. Then we calculate the internal moment using Eq. (A10)~~(A10)~~,

$$\int_A \sigma_x z \mathrm{d}A = EI\left(1/R - 1/R_{\mathrm{ph}}\right), \tag{A11}$$

with

~~condition and moment free conditions~~balance conditions to Eq. (A10)~~(A19), namely~~ ~~$\int_A \sigma_x \mathrm{d}A = 0$ and $\int_A \sigma_x z \mathrm{d}A = EI\left(1/R - 1/R_{\mathrm{ph}}\right)$, we get $z_{\mathrm{n}}/R = \int_A \varepsilon_{\mathrm{ph}}(z)\mathrm{d}A/A$, with~~

where we have taken the centroid of the cross-section as the origin of the coordinate system.

Field Code Changed

Field Code Changed

Field Code Changed

Formatted: Check spelling and grammar

APPENDIX B: Time response of the cantilever's tip displacement and photo-curvature for $t_i / t_d = 100000$

As shown in Fig. 6, when the diffusion is much faster than the vibration, the photo curvature acts like a step-function excitation.

Equation Chapter (Next) Section 1

APPENDIX C: The scaling of the radius of curvature of a hydrogel oscillator

To estimate the radius of curvature of a hydrogel oscillator due to inhomogeneous water concentration along the thickness, we simply consider water diffuses up to certain diffusion distance $h_d \sim \sqrt{DT_p}$, where D is the diffusivity of water molecules in the hydrogel and T_p is the period of the vibration. The spontaneous photo strain is assumed to be ε_0 on the shined surface $z = h/2$, linearly decreases with z, and reach zero at $z = h/2 - h_d$, i.e.

$$\varepsilon_{\text{ph}}(z) \sim \left[\left(\frac{h}{2} - h_d \right) \right], \quad h/2 - h_d < z < h/2 \tag{C1}$$

Using Eq. (3) and we have

$$1/R_{\text{ph}} = -\int_A \varepsilon_{\text{ph}}(z) z \mathrm{d}A / I \sim \sim \sim \sim \sim \sqrt{DT_p}, \tag{C2}$$

where ε_0 is determined by the photo chemical potential $\mu_{\text{ph}} / k_{\text{B}}T$, and we have assumed $h_d < h$. Therefore, the spontaneous radius of curvature scales with the square of the thickness, $R_{\text{ph}} \sim h^2$, is inversely proportional to the diffusion thickness $\sqrt{DT_p}$, and nonlinearly depends on the photo chemical potential $\mu_{\text{ph}} / k_{\text{B}}T$.

APPENDIX D: The estimation of the damping coefficient

For a slender structure with length L and width b vibrating with velocity v, the Reynolds number can be calculated as Re = $\rho_w v b / \mu_w$. Given the density of water $\rho_w = 10^3 kg/m^3$, viscosity of water $\mu_w = 8.9 \times 10^{-4} Pa \cdot s$, $b = 10^{-3}$ mm and velocity $v = 10^{-3} m/s$, we can know that the fluid has a low Reynold number, Re ≈ 1. The damping coefficient c can be calculated from the drag force F_d, $c = F_d / Lv$. For a low-Reynolds-number fluid, the drag coefficient defined as $c_d = 2F_d / \rho_w v^2 L b$ equals A_d/Re, with A_d a constant coefficient depending on the cross-section of the slender structure [47]. Therefore, the damping coefficient is calculated as $c = A_d \mu_w / 2$. When the cross-section is circular, A_d is 24. Here we just generically set A_d to be 10. Therefore, the damping coefficient is estimated to be $4.45 \times 10^{-3} Pa \cdot s$.

Equation Chapter (Next) Section 1

APPENDIX E: The scaling of the work done and damping energy of the mass-spring-damper system

When the excitation velocity $\sqrt{m/k} / \tau$ is limited to less than 0.1, the normalized vabriation frequency is almost a constant. Using Eq. (9), the maximum applied force F_{max} is proportional to $F_\infty \sqrt{m/k} / \tau$, namely, $F_{\text{max}} \sim \bar{k} / \tau$. Therefore, we have

$$W_f = \int_0^{T_p} F \sim \sim \sqrt{m/k}/\tau \left(kA_x/F_\infty\right). \quad \text{(E1)}$$

The damping energy is obtained as

$$W_\alpha = \int_0^{T_p} \alpha \sim \sim \sim \sqrt{km} \left(kA_x/F_\infty\right)^2. \quad \text{(E2)}$$

References

[1] M. A. C. Stuart, W. T. Huck, J. Genzer, M. Müller, C. Ober, M. Stamm, G. B. Sukhorukov, I. Szleifer, V. V. Tsukruk, and M. Urban, *Emerging Applications of Stimuli-Responsive Polymer Materials*, Nat. Mater. **9**, 101 (2010).

[2] M. Rogóż, H. Zeng, C. Xuan, D. S. Wiersma, and P. Wasylczyk, *Light-driven Soft Robot Mimics Caterpillar Locomotion in Natural Scale*, Adv. Opt. Mater. **4**, 1689 (2016).

[3] G. Li, X. Chen, F. Zhou, Y. Liang, Y. Xiao, X. Cao, Z. Zhang, M. Zhang, B. Wu, and S. Yin, *Self-Powered Soft Robot in the Mariana Trench*, Nature **591**, 66 (2021).

[4] Y. Kim, H. Yuk, R. Zhao, S. A. Chester, and X. Zhao, *Printing Ferromagnetic Domains for Untethered Fast-Transforming Soft Materials*, Nature **558**, 274 (2018).

[5] H. Shahsavan, A. Aghakhani, H. Zeng, Y. Guo, Z. S. Davidson, A. Priimagi, and M. Sitti, *Bioinspired Underwater Locomotion of Light-Driven Liquid Crystal Gels*, Proc. Natl. Acad. Sci. **117**, 5125 (2020).

[6] L. Hines, K. Petersen, G. Z. Lum, and M. Sitti, *Soft Actuators for Small-scale Robotics*, Adv. Mater. **29**, 1603483 (2017).

[7] Y. Zhao, C. Xuan, X. Qian, Y. Alsaid, M. Hua, L. Jin, and X. He, *Soft Phototactic Swimmer Based on Self-Sustained Hydrogel Oscillator*, Sci. Robot. **4**, (2019).

[8] Y. Kim, J. van den Berg, and A. J. Crosby, *Autonomous Snapping and Jumping Polymer Gels*, Nat. Mater. 1 (2021).

[9] K. Li, X. Su, and S. Cai, *Self-Sustained Rolling of a Thermally Responsive Rod on a Hot Surface*, Extreme Mech. Lett. **42**, 101116 (2021).

[10] H. Zeng, M. Lahikainen, L. Liu, Z. Ahmed, O. M. Wani, M. Wang, H. Yang, and A. Priimagi, *Light-Fuelled Freestyle Self-Oscillators*, Nat. Commun. **10**, 1 (2019).

[11] Z.-Z. Nie, B. Zuo, M. Wang, S. Huang, X.-M. Chen, Z.-Y. Liu, and H. Yang, *Light-Driven Continuous Rotating Möbius Strip Actuators*, Nat. Commun. **12**, 1 (2021).

[12] H. Zhu, B. Xu, Y. Wang, X. Pan, Z. Qu, and Y. Mei, *Self-Powered Locomotion of a Hydrogel Water Strider*, Sci. Robot. **6**, (2021).

[13] K. Korner, A. S. Kuenstler, R. C. Hayward, B. Audoly, and K. Bhattacharya, *A Nonlinear Beam Model of Photomotile Structures*, Proc. Natl. Acad. Sci. **117**, 9762 (2020).

[14] L. Yang, L. Chang, Y. Hu, M. Huang, Q. Ji, P. Lu, J. Liu, W. Chen, and Y. Wu, *An Autonomous Soft Actuator with Light-driven Self-sustained Wavelike Oscillation for Phototactic Self-locomotion and Power Generation*, Adv. Funct. Mater. **30**, 1908842 (2020).

[15] Z. Hu, Y. Li, and J. Lv, *Phototunable Self-Oscillating System Driven by a Self-Winding Fiber Actuator*, Nat. Commun. **12**, 1 (2021).

[16] T. J. White, N. V. Tabiryan, S. V. Serak, U. A. Hrozhyk, V. P. Tondiglia, H. Koerner, R. A. Vaia, and T. J. Bunning, *A High Frequency Photodriven Polymer Oscillator*, Soft Matter **4**, 1796 (2008).

[17] X. He, M. Aizenberg, O. Kuksenok, L. D. Zarzar, A. Shastri, A. C. Balazs, and J. Aizenberg, *Synthetic Homeostatic Materials with Chemo-Mechano-Chemical Self-Regulation*, Nature **487**, 214 (2012).
[18] A. W. Hauser, S. Sundaram, and R. C. Hayward, *Photothermocapillary Oscillators*, Phys Rev Lett **121**, 158001 (2018).
[19] P. R. Buskohl and R. A. Vaia, *Belousov-Zhabotinsky Autonomic Hydrogel Composites: Regulating Waves via Asymmetry*, Sci. Adv. **2**, e1600813 (2016).
[20] A. Chakrabarti, G. P. T. Choi, and L. Mahadevan, *Self-Excited Motions of Volatile Drops on Swellable Sheets*, Phys. Rev. Lett. **124**, 258002 (2020).
[21] R. K. Manna, O. E. Shklyaev, and A. C. Balazs, *Chemical Pumps and Flexible Sheets Spontaneously Form Self-Regulating Oscillators in Solution*, Proc. Natl. Acad. Sci. **118**, (2021).
[22] S. Maeda, Y. Hara, T. Sakai, R. Yoshida, and S. Hashimoto, *Self-walking Gel*, Adv. Mater. **19**, 3480 (2007).
[23] R. Yoshida and T. Ueki, *Evolution of Self-Oscillating Polymer Gels as Autonomous Polymer Systems*, NPG Asia Mater. **6**, e107 (2014).
[24] B. E. Treml, R. N. McKenzie, P. Buskohl, D. Wang, M. Kuhn, L.-S. Tan, and R. A. Vaia, *Autonomous Motility of Polymer Films*, Adv. Mater. **30**, 1705616 (2018).
[25] D. Corbett, C. Xuan, and M. Warner, *Deep Optical Penetration Dynamics in Photobending*, Phys. Rev. E **92**, 013206 (2015).
[26] A. H. Gelebart, G. Vantomme, E. W. Meijer, and D. J. Broer, *Mastering the Photothermal Effect in Liquid Crystal Networks: A General Approach for Self-Sustained Mechanical Oscillators*, Adv Mater **29**, (2017).
[27] K. Kumar, C. Knie, D. Bleger, M. A. Peletier, H. Friedrich, S. Hecht, D. J. Broer, M. G. Debije, and A. P. Schenning, *A Chaotic Self-Oscillating Sunlight-Driven Polymer Actuator*, Nat Commun **7**, 11975 (2016).
[28] S. Serak, N. Tabiryan, R. Vergara, T. J. White, R. A. Vaia, and T. J. Bunning, *Liquid Crystalline Polymer Cantilever Oscillators Fueled by Light*, Soft Matter **6**, 779 (2010).
[29] K. M. Lee, M. L. Smith, H. Koerner, N. Tabiryan, R. A. Vaia, T. J. Bunning, and T. J. White, *Photodriven, Flexural–Torsional Oscillation of Glassy Azobenzene Liquid Crystal Polymer Networks*, Adv. Funct. Mater. **21**, 2913 (2011).
[30] A. H. Gelebart, D. Jan Mulder, M. Varga, A. Konya, G. Vantomme, E. W. Meijer, R. L. B. Selinger, and D. J. Broer, *Making Waves in a Photoactive Polymer Film*, Nature **546**, 632 (2017).
[31] K. Li and S. Cai, *Modeling of Light-Driven Bending Vibration of a Liquid Crystal Elastomer Beam*, J. Appl. Mech. **83**, 031009 (2016).
[32] G. Vantomme, A. H. Gelebart, D. J. Broer, and E. W. Meijer, *Self-sustained Actuation from Heat Dissipation in Liquid Crystal Polymer Networks*, J. Polym. Sci. Part Polym. Chem. **56**, 1331 (2018).
[33] D. Zhao and Y. Liu, *Photomechanical Vibration Energy Harvesting Based on Liquid Crystal Elastomer Cantilever*, Smart Mater. Struct. **28**, 075017 (2019).
[34] O. Makarenkov and J. S. Lamb, *Dynamics and Bifurcations of Nonsmooth Systems: A Survey*, Phys. Nonlinear Phenom. **241**, 1826 (2012).
[35] W. M. Hartmann, *The Dynamically Shifted Oscillator*, Am. J. Phys. **54**, 28 (1986).

[36] Y. Chen and L. Jin, *Snapping-Back Buckling of Wide Hyperelastic Columns*, Extreme Mech. Lett. 100600 (2019).
[37] A. Li, L. Ma, D. Keene, J. Klingel, M. Payne, and X. Wang, *Forced Oscillations with Linear and Nonlinear Damping*, Am. J. Phys. **84**, 32 (2016).
[38] W. Hong, X. Zhao, J. Zhou, and Z. Suo, *A Theory of Coupled Diffusion and Large Deformation in Polymeric Gels*, J. Mech. Phys. Solids **56**, 1779 (2008).
[39] C. Xuan and L. Jin, *Concurrent Reaction and Diffusion in Photo-Responsive Hydrogels*, J. Mech. Phys. Solids **124**, 599 (2019).
[40] A. Mourran, H. Zhang, R. Vinokur, and M. Möller, *Soft Microrobots Employing Nonequilibrium Actuation via Plasmonic Heating*, Adv. Mater. **29**, 1604825 (2017).
[41] See Supplemental Material at [URL Inserted by Publisher] for videos exhibiting photo-driven self-excited hydrogel oscillators with amplitude increase and decrease.
[42] J. P. Den Hartog, *Mechanical Vibrations* (Courier Corporation, 1985).
[43] P. J. Flory and J. Rehner Jr, *Statistical Mechanics of Cross-linked Polymer Networks I. Rubberlike Elasticity*, J. Chem. Phys. **11**, 512 (1943).
[44] P. J. Flory, *Principles of Polymer Chemistry* (Cornell University Press, 1953).
[45] P. J. Flory, *Thermodynamics of High Polymer Solutions*, J. Chem. Phys. **10**, 51 (1942).
[46] M. Warner, C. D. Modes, and D. Corbett, *Suppression of Curvature in Nematic Elastica*, Proc. R. Soc. Math. Phys. Eng. Sci. **466**, 3561 (2010).
[47] A. M. Jones and J. G. Knudsen, *Drag Coefficients at Low Reynolds Numbers for Flow Past Immersed Bodies*, AIChE J. **7**, 20 (1961).

Figures and Tables

Figure 1.

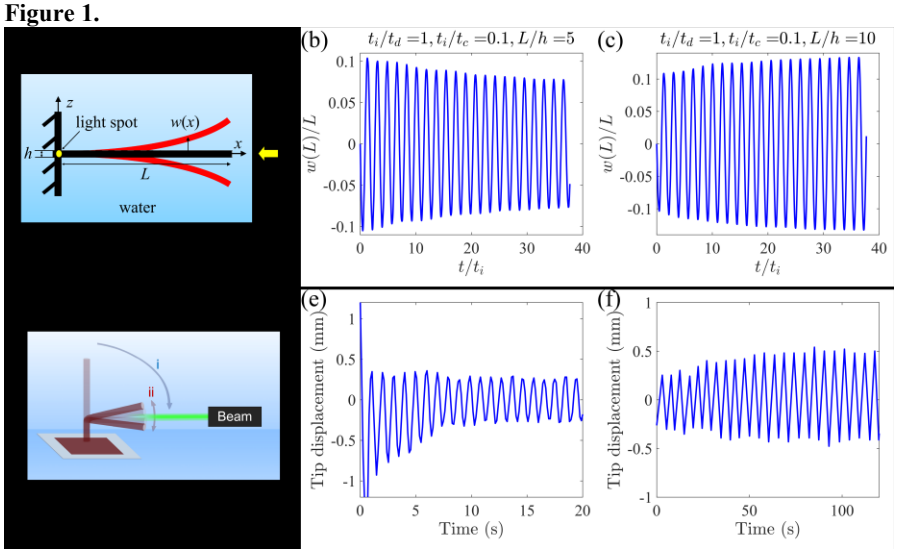

FIG. 1 (a) Schematic of self-excited oscillation of a hydrogel cantilever in response to constant light radiation. (b), (c) Time response of the cantilever's tip displacement for different length-to-thickness ratios. The tip amplitude decreases with time for $L/h = 5$ and increases for $L/h = 10$. (d) Schematics of the experimental setup for self-excited oscillation of a photo-thermally responsive hydrogel. Time response of the tip displacement of a (e) thick (h=0.9mm, L/h = 18.9), and (f) thin (h=0.56mm, L/h = 30.4) cantilever of length L=17mm.
(Note: 2 columns are used for this figure.)

Figure 2.

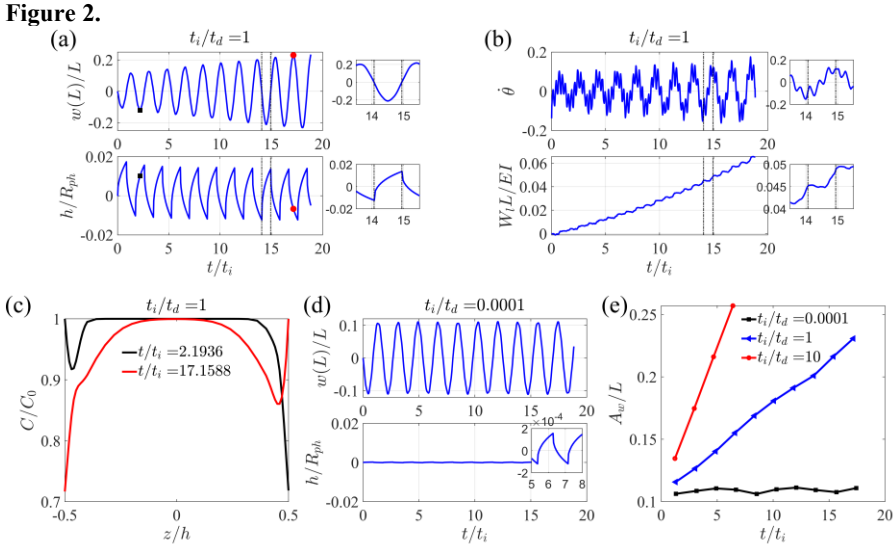

FIG. 2 (a), (d) Time response of the cantilever's tip displacement $w(L)/L$ and photo-curvature h/R_{ph} for different normalized diffusivities $t_{\mathrm{i}}/t_{\mathrm{d}}=1,\ 0.0001$, respectively. (b) Time response of the change rate of the bending angle $\dot{\epsilon}$ at $x=d_{ph}$ and the work done to the cantilever $W_l L/EI$. (c) Water concentration depth profiles at different time $t/t_{\mathrm{i}}=2.19$ and $t/t_{\mathrm{i}}=17.15$, corresponding to the valley and peak of tip displacements indicated by the black square and red circle in (a). (e) Amplitude of the tip displacement as a function to time for different $t_{\mathrm{i}}/t_{\mathrm{d}}$.

(Note: 2 columns are used for this figure.)

Figure 3.

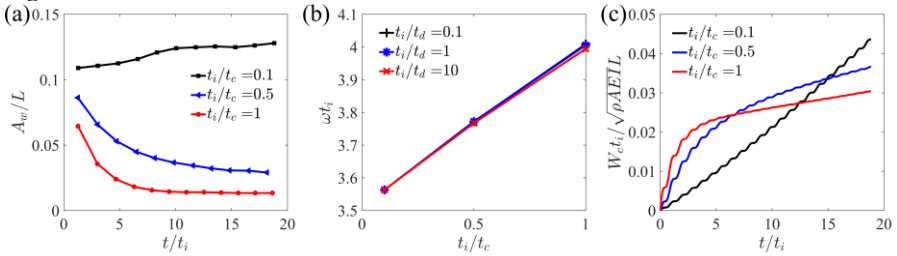

FIG. 3 (a) Time response of the amplitude of the tip displacement for different normalized damping factors. (b) Influence of the normalized damping factor and diffusivity on the cantilever oscillation frequency. (c) Time response of the energy loss for different damping factors.

(Note: 2 columns are used for this figure.)

Figure 4.

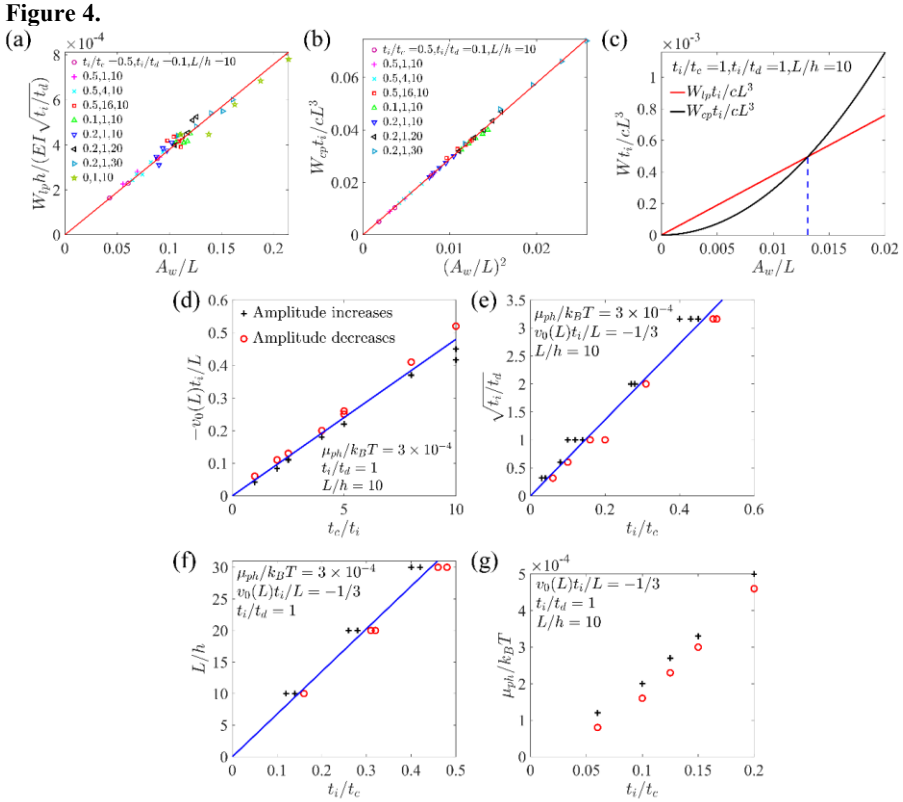

FIG. 4 (a) Normalized work done $W_{lp}h/\left(EI\sqrt{t_i/t_d}\right)$ as a function of the normalized tip amplitude A_w/L, and (b) normalized damping energy $W_{cp}t_i/cL^3$ as a function of the square of the tip amplitude $\left(A_w/L\right)^2$ for a wide range of t_i/t_c, t_i/t_d and L/h. (c) Normalized work input and energy dissipation as a function of the normalized tip amplitude A_w/L. Boundaries between amplitude increase and decrease in phase planes of different dimensionless parameters: (d) in the phase plane of t_c/t_i and $v_0(L)t_i/L$ under constant μ_{ph}/k_BT, t_i/t_d and L/h; (e) in the phase plane of t_i/t_c and $\sqrt{t_i/t_d}$ under constant μ_{ph}/k_BT, $v_0(L)t_i/L$ and L/h; (f) in the phase plane of t_i/t_c and L/h under constant μ_{ph}/k_BT, $v_0(L)t_i/L$ and t_i/t_d; (g) in the phase plane of t_i/t_c and μ_{ph}/k_BT under constant $v_0(L)t_i/L$, t_i/t_d and L/h. All the symbols are numerical results, and the lines are fitting results from the scaling analysis.
(Note: 2 columns are used for this figure.)

Figure 5.

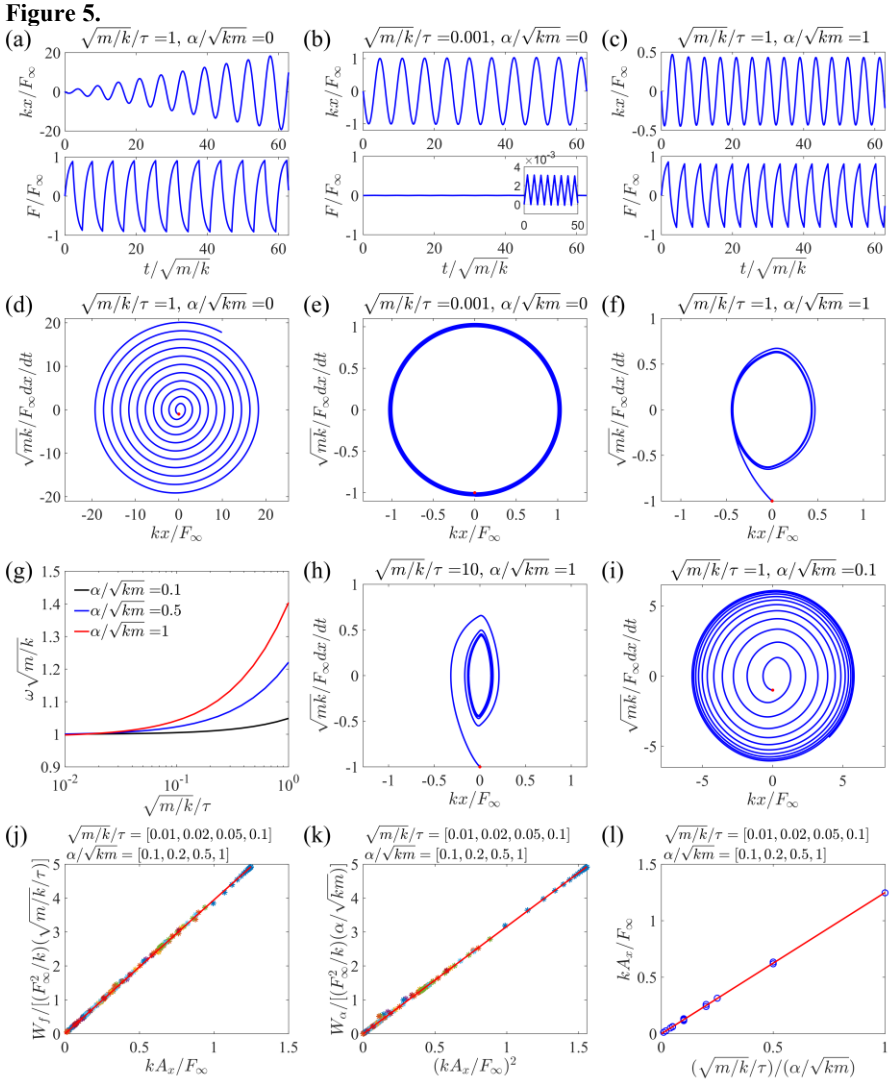

FIG. 5 (a), (b) Undamped time response of the displacement and the excitation force for time-scale ratios $\sqrt{m/k}/\tau = 1$ and $\sqrt{m/k}/\tau = 0.001$, respectively. (d), (e) Undamped phase plane for time scale $\sqrt{m/k}/\tau = 1$ and $\sqrt{m/k}/\tau = 0.001$, respectively. (c) Damped time response of the displacement and the excitation force. (f) (h) (i) Damped phase plane for different normalized excitation velocities and damping factors. (g) Dependence of vibration frequency $\omega\sqrt{m/k}$ on the normalized excitation velocity $\sqrt{m/k}/\tau$ under

different normalized damping factors $\alpha/\sqrt{km}$. (j) Normalized work done as a function of the normalized vibration amplitude, and (k) normalized damping energy as a function of the square of the vibration amplitude for a wide range of $\sqrt{m/k}/\tau$ and $\alpha/\sqrt{km}$. (l) Normalized stable amplitude as a function of the ratio between the excitation velocity $\sqrt{m/k}/\tau$ and normalized damping factors $\alpha/\sqrt{km}$. In (j-l) all the symbols are numerical results under different combinations of data sets $\sqrt{m/k}/\tau = [0.01, 0.02, 0.05, 0.1]$ and $\alpha/\sqrt{km} = [0.1, 0.2, 0.5, 1]$, and the lines are fitting results from the scaling analysis.
(Note: 2 columns are used for this figure.)

Figure 6.

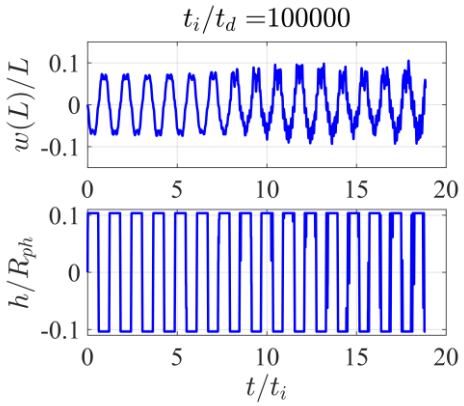

FIG. 6 Time response of the cantilever's tip displacement and photo-curvature for the normalized diffusivity $t_i/t_d = 100000$. The curvature behaves like a step function. The frequency is higher than that with a smaller normalized diffusivity.
(Note: 1 column is used for this figure.)